Research Article

Gold semicontinuous thin-film-coated mesoporous TiO_2 for SERS substrates

M. Mercedes Zalduendo[1] · Paula Y. Steinberg[1] · Tomás Prudente[2] · Emiliano J. Di Liscia[3] · Josefina Morrone[1] · Paula C. Angelomé[1] · Cristián Huck-Iriart[2]

Received: 24 July 2020 / Accepted: 6 October 2020

Abstract
In this work, the preparation and thermal evolution of sputtered semicontinuous gold thin films obtained over ordered mesoporous TiO_2 films are presented. The controlled surface topography of the ordered mesoporous TiO_2 substrate was used as template for obtaining plasmonic hotspots for Surface Enhanced Raman Spectroscopy (SERS) applications. Plasmonic thin film was obtained by Au sputtering when film thickness was under circa 10 nm. Above this value, the porosity effects from the substrate were lost and Raman signal enhancement with it. Moreover, heat treatment was explored in order to obtain gold nanoislands that can also provide very efficient Raman enhancement. Hence, a very straightforward synthesis procedure is presented for sensing application, even for large scale production.

Keywords SERS · Mesoporous oxide thin films · Plasmonic films · Sputtering

1 Introduction

Surface-enhanced Raman scattering (SERS) spectroscopy is a sensitive technique to characterize, detect and, in some cases, quantify different types of analytes at very low concentrations [1, 2]. SERS based sensing is currently routinely used in several analytical applications ranging from the detection of explosive agents and drugs, to the prevention of documents, medicines and food products falsification, the detection of food contaminants and the quality control [3–5]. Other interesting reported applications of SERS based sensing include the areas of personalized diagnostics [6], immunoassay platforms [7], bioimaging and biosensing [8–10], biomedicine [11], detection of heavy metal anions and other environmental contaminants [12, 13], among others [14–16].

Most common SERS sensors are built using metallic nanoparticles (NPs) such as gold [17], silver [18], and copper [19], either in solution or supported onto substrates. The enhancement of inelastic scattering by the plasmonic effect in the metallic nanosized particles and films are related to the size, shape, morphology, inter-particle distance and arrangement of the plasmonic nanostructure [20–23].

Mesoporous oxide thin films obtained by the sol–gel process are already employed to design diverse SERS sensors [24]. Ordered mesoporous materials exhibit high porosity where the pore size and order can be modified

Electronic supplementary material The online version of this article (https://doi.org/10.1007/s42452-020-03635-9) contains supplementary material, which is available to authorized users.

✉ Paula C. Angelomé, angelome@cnea.gov.ar; ✉ Cristián Huck-Iriart, chuck@unsam.edu.ar | [1]Gerencia Química & Instituto de Nanociencia y Nanotecnología, Centro Atómico Constituyentes, Comisión Nacional de Energía Atómica, CONICET, Av. Gral. Paz 1499, 1650 San Martín, Buenos Aires, Argentina. [2]Laboratorio de Cristalografía Aplicada, Escuela de Ciencia Y Tecnología, Universidad Nacional de San Martín (UNSAM), Campus Miguelete, 25 de Mayo y Francia, 1650 San Martín, Buenos Aires, Argentina. [3]Departamento de Materia Condensada, GAIyANN, Comisión Nacional de Energía Atómica, Av. Gral. Paz 1499, 1650 San Martín, Buenos Aires, Argentina.

Published online: 10 October 2020

by using different types of surfactants and by controlling the processing variables such as temperature, humidity, catalyst, etc. [25]. Mesoporous films offer the possibility to support metal NPs thus avoiding their destabilization in solution. Moreover, NPs remain in contact with the medium thanks to the porosity. Different architectures were proposed for the combination of these two materials: metal NPs inside the mesostructured oxide film [26–29], metal NPs placed between the oxide film and the substrate [28–32], and metallic NPs or films in the air-oxide film interface [33–38]. Alternatively, metallic particles covered with a mesoporous shell can be deposited onto substrates to prepare films for SERS sensing [39, 40]. While these kinds of sensors present very attractive features such as high chemical and mechanical stability, each architecture displays different sensing capabilities. For example, high spatial homogeneity of the SERS signal can be obtained when NPs are synthesized inside the mesoporous oxide film [27–29], while the mesoporous oxide film can be used as an active part of the sensor giving selectivity to the detection [30–32]. Nevertheless, when the plasmonic material is placed inside the mesoporous oxide film or in the substrate-oxide interface, Raman enhancement of the sensor may be attenuated because the SERS signal relies on NPs surface availability, NPs proximity and diffusion of the analyte within the pores. In fact, previous studies of NPs grown or deposited over mesoporous oxide films showed higher SERS and localized surface plasmon resonance (LSPR) sensibility [33, 34, 38] compared to the other architectures. However, in this type of design the plasmonic material is usually more unstable.

In order to obtain metallic nanosized particles without capping agents, sputtering methods have been studied over different substrates or arrangements [41–46]. Recently, Bonyár and coworkers prepared a series of gold nanoisland obtained by sputtering over SiO_2 substrates followed by thermal treatment [47]. These authors analyzed the LSPR and SERS based sensing properties, as a function of the arrangement obtained after thermal annealing. Moreover, Pavaskar et al. produced Au and Ag island-like plasmonic thin films *ca.* 5 nm thick over transmission electron microscopy grids and simulated their Raman enhancement. They concluded that hot spots were located between small nm-sized gaps which dominate the electromagnetic response of those films [48]. One particular case of substrate for metal layer formation are mesoporous oxides. This type of substrates has been used to support the plasmonic material in their interface with air and some examples can be found in literature such as Ag over TiO_2 mesoporous thin films [35] and Au over SiO_2 mesoporous thin films [36–38]. For the latter case, Murai and coworkers showed that Au thin film properties strongly depend on the rugosity of the SiO_2 film used as substrate. However, a thin layer of Cr (< 0.3 nm) was used to ensure Au adhesivity over the SiO_2 film. Thus, despite there are several examples in literature in which metallic nanostructures were synthesized over different substrates and used for SERS or LSPR based sensors [49–52], the use of mesoporous oxides as agents for nanostructuring noble metal thin films was not described.

In this work, mesoporous and non-mesoporous oxide thin films were used as substrate for Au plasmonic thin film deposition. The obtained systems, whose characteristics depend on the oxide layer structure and chemical nature, were tested as SERS based sensors for detection for different organic probes. The effect of different parameters, including: metallic layer thickness, oxide layer composition and porosity and the thermal treatment, over the structural properties and the sensing capabilities of the Au layer were determined. The proposed synthetic path allows obtaining, in simple steps, a variety of SERS sensors whose applications will be determined by their differential characteristics.

2 Materials and methods

2.1 Materials

Titanium tetrachloride ($TiCl_4$) and tetraetoxysilane (TEOS) were supplied by Merck, while Pluronic F127 ($HO\text{-}(CH_2CH_2O)_{106}(CH_2CH(CH_3)\text{-}O)_{70}(CH_2CH_2O)_{106}OH$), titanium(IV) ethoxide (TEOT) and rhodamine 6G (R6G) were supplied by Sigma-Aldrich and para-nitrothiophenol (pNTP) (80%) by Acros-Organics. Na_2HPO_4 (Biopack) and NaH_2PO_4 (Merck) were used to prepare phosphate buffer saline (PBS) 0.5 M pH = 7.4. Nitric acid (HNO_3) was purchased from Anedra and chloridric acid (HCl) from Merck. Pure grade ethanol and Milli-Q water were used as solvents. All chemicals were used as received.

2.2 Oxide thin films

Mesoporous oxide thin films were produced according to previously reported methods [53, 54]. For non-mesoporous titania films a solution was prepared by dropping TEOT, under stirring, in a solution containing HNO_3, H_2O and ethanol. The final molar ratios were 1:0.2:1.4:44.8, respectively. The mixture was stirred for 2 h at room temperature. Mesoporous thin films were produced via the Evaporation-Induced Self-Assembly (EISA) strategy [55] using an inorganic precursor ($TiCl_4$) and a template (Pluronic F127) in ethanol. Films were deposited from a solution prepared with $TiCl_4$, EtOH, F127 and H_2O, with 1:40:0.005:10 molar ratio. Non mesoporous silica films

were produced from a solution containing TEOS, HCl, ethanol and H_2O with 1:0.008:40:10 molar ratio. While mesoporous silica films were obtained from a mixture of TEOS, HCl, ethanol, H_2O and F127 with 1:0.008:40:10:0.005 molar ratio, also using the EISA approach. This solution was aged for at least 48 h prior to use.

For the four systems, each solution was deposited onto clean glass slides by dip-coating (withdrawal speed: 1 mm s^{-1}). Once deposited onto the substrates, the films were placed in a chamber at 50% relative humidity (fixed with a $Ca(NO_3)_2$ saturated aqueous solution) for 24 h. Then, they were stabilized applying a two step thermal treatment: 24 h at 60 °C and 24 h at 130 °C. Finally, the films were calcined for 2 h at 350° C (1 °C per minute ramp).

Non-mesoporous titania thin films were labeled TNM while mesoporous titania thin films were named TF (F indicates the template, Pluronic F127). The same code was used for silica films, that were named SNM and SF.

2.3 Au sputtering

Before Au deposition, oxide thin films were cut into regular pieces of about 1×1 cm^2 and thoroughly rinsed with water and ethanol to guarantee surface cleanliness. Au films were deposited by sputtering using a Quorum Q300T D equipment with Ar plasma. Sputtering exposure times were varied between 5 and 20 s in order to obtain Au films of different thicknesses. Alternatively, the samples were thermally treated for 1 h at a final temperature of 300 °C using a 5 °C/min heating rate from room temperature.

Systems were named TNM/Au*X*nm or SNM/Au*X*nm and TF/Au*X*nm or SF/Au*X*nm, where *X*nm represents a Au film of *X* nm thickness. After thermal treatment, the final temperature was added at the end of the sample name.

2.4 Characterization

The surface of the samples was observed by scanning electron microscopy (SEM) using a Carl-Zeiss SUPRA 40 microscope.

X-ray reflectometry (XRR) was used to determine Au layer thickness and the mesoporous oxides porosities [56]. Measurements were performed with a Panalytical Empyrean X-Ray diffractometer with an incident beam of Cu K_α radiation (1.54 Å).

UV–visible spectra were acquired using an Agilent 8453 spectrophotometer. Samples were placed in an appropriately designed sample holder that allows measurement in transmission mode.

For SERS measurements, pNTP and R6G were chosen as analytes. pNTP presents a thiol group that covalently bonds to Au and provides strong and easily recognizable Raman signals [28]. Thus, it was used as the test analyte for the characterization of all the samples. For this analyte, samples were immersed for 1 h in 1 mL of pNTP 4×10^{-4} M (solvent: PBS) at 4 °C. After incubation, samples were rinsed with water and air-dried. Under these conditions, a full coverage of the available Au surface is expected. R6G, on the other hand, is a non-interacting analyte that was used for preliminary tests. In this case, a 7×10^{-6} M R6G ethanolic solution was deposited by drop casting directly onto the sensors, no rinsing step was performed.

SERS spectra were recorded using a Horiba LabRAM HR Raman with confocal microscope (Horiba JobinYvon), equipped with a 632.8 nm laser and a 600 grooves mm^{-1} grating. Appropriate filter optics were used to avoid probes degradation. Measurements were performed using a $100 \times$ objective (NA 0.9) and confocality mode with a 100 µm pinhole. Spectra were taken from at least 10 different points in each sample, using acquisition times from 5 to 30 s (1 scan).

3 Results and discussion

3.1 Synthesized systems

Two different TiO_2 films were used to sputter Au on their surface: TiO_2 mesoporous films (TF) and TiO_2 non-mesoporous films (TNM). TF system presented a thickness of 140 ± 10 nm and a porosity of 45 ± 5%, as obtained from XRR analysis (see Fig. S1, SI). The surface of the TF system can be observed in Fig. S1 in which pores of diameter 8 ± 1 nm can be easily identified. On the other hand, TNM system presented a smooth surface (Fig. S1) and a thickness of 60 ± 6 nm. These results are in agreement with previously reported data for similar systems [29, 56, 57].

Sputtering times from 5 to 15 s were used to deposit Au over these film's surfaces. Gold film thicknesses over TiO_2 films increased from 5 to 15 nm with sputtering time. Optical images of all obtained platforms are shown in Fig. S2 (SI): a color change from blue to golden can be distinguished as sputtering time increments. This was also observed for Au films deposited onto glass and corresponds to a transition from a discontinuous metallic film to a continuous one, as the sputtering time is incremented [58–60].

The texture of the gold layer deposited onto the TiO_2 oxides, observed by SEM, are presented in Fig. 1. In the case of TNM films, SEM images show a polycrystalline continuous Au film for all sputtering times. For mesoporous TF films, on the other hand, nanostructured Au films with homogeneously distributed holes are observed. Therefore, these results indicate that modifying the TiO_2 surface topology with an ordered mesoporous motif allows templating Au condensation and structuration. Moreover,

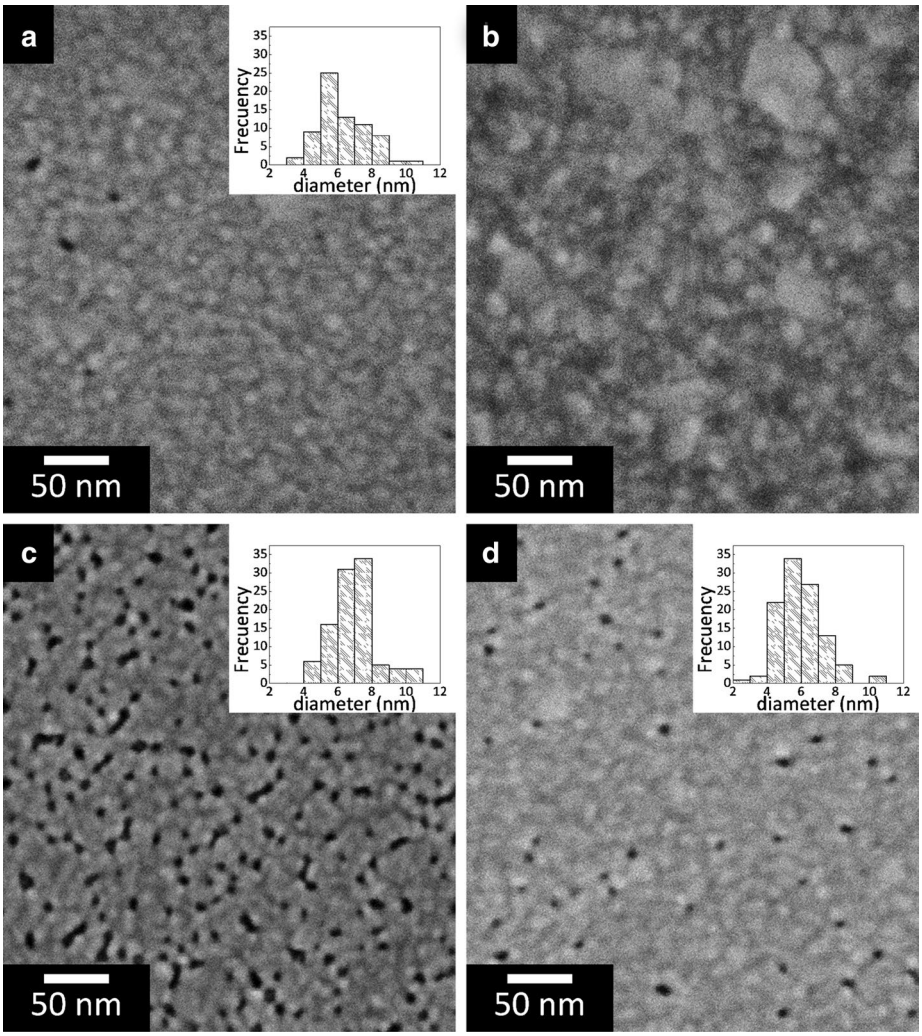

Fig. 1 SEM images of **a** TNM/Au5nm, **b** TNM/Au8nm, **c** TF/Au5nm, and **d** TF/Au8nm systems. Insets correspond to holes size distribution

Fig. 1c and d show that the holes in the Au film present a diameter of *ca*. 6 nm, a value close to the substrate pore average diameter (8 nm) [57]. Thus, the obtained holes seem to be derived from TiO_2 pores partially coated with Au. When a thicker film of Au was grown, no significant differences in the obtained metallic film were observed between TNM/Au15nm and TF/Au15nm systems. This observation can be explained taking into account that the gold film is expected to fully cover the TiO_2 surface under this deposition condition [37].

According to bibliography, nanosized islands are formed when Au thin films are exposed to a heating treatment [47, 49, 61]. Thus, in order to compare Au film stability and sensing properties, samples were treated for 1 h at 300 °C as explained in the experimental section. After thermal treatment a change in samples color is readily observed (see Fig. S2, SI): an intense pink-violet color is clearly developed. Moreover, the UV–visible spectra change: from having ill-defined bands, typical of plasmonic metallic films, to present well-defined single bands centered at around 600 nm, typical of Au NPs LSPR (see Fig. S3, SI). The SEM images presented in Fig. 2 confirm the NPs formation after heat treatment. In these images, NPs are seen as bright asymmetrical features randomly distributed onto the surface. For the TNM/Au5nm-300 system, a smooth surface can be recognized below the NPs: the TNM surface. On the other hand, the porous TiO_2 surface can be identified below the NPs in TF/Au5nm-300 system: the pores are seen as darker circles, with the typical arrangement of F127 templated oxides. NPs size distribution is broad, independently on the oxide film used as support (TNM or TF). Though NPs average size is similar (approximately 60 nm in diameter), there is a greater number of larger NPs in the TNM system. Likewise, the calculated NPs area density is 80 ± 5 NPs/μm^2 for the TNM/Au5nm-300 system and 100 ± 5 NPs/μm^2 for the TF/Au5nm-300 system. Therefore, no clear effect of oxide films surface topology over the NPs formation was observed.

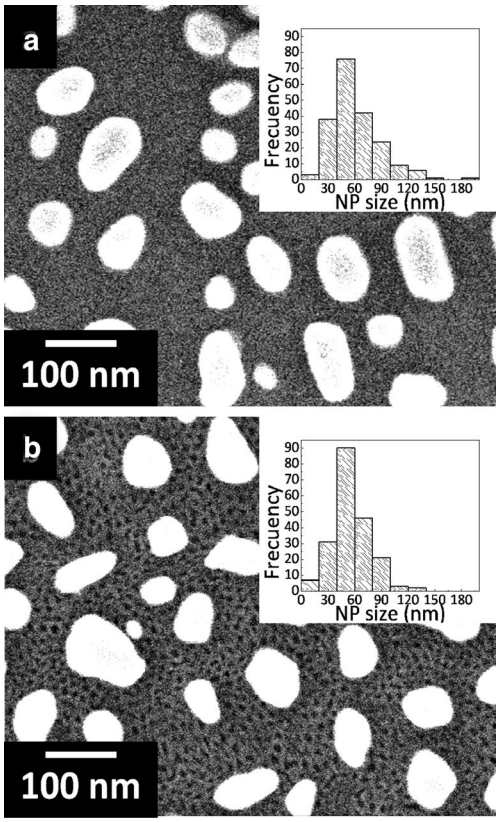

Fig. 2 SEM images of **a** TNM/Au5nm-300, and **b** TF/Au5nm-300 systems. Insets correspond to NPs size distribution

3.2 Systems stability

For SERS sensing capability studies, samples were immersed into diluted pNTP aqueous solutions and rinsed with water after incubation. It is important to highlight that, in the literature, this type of systems, in which the metal NPs or metal film are deposited onto a substrate, are usually incubated by drying a drop of analyte solution. Therefore, the methodology proposed in this work allows not only to study the SERS effect, but also to analyze the adhesion of the Au film and the effects of a corrosive solution over the sensors structure.

After incubation, no optical changes were observed for Au films deposited over TiO_2 films (Fig. S2, SI). A comparative study was carried out with Au layers deposited over SiO_2 films. In this case, the Au film detached after incubation, as can be seen in Fig. S2, SI. These results indicate a better adhesion of the Au film over TiO_2 in comparison with SiO_2 films. Interestingly, no adhesion layer was needed to maintain Au attached to the TiO_2 film, a feature that can be attributed to metal/oxide interactions and the oxide chemical stability [62, 63].

Figure 3a, b show SEM images of TNM/Au8nm and TF/Au8nm samples after incubation with the SERS probe.

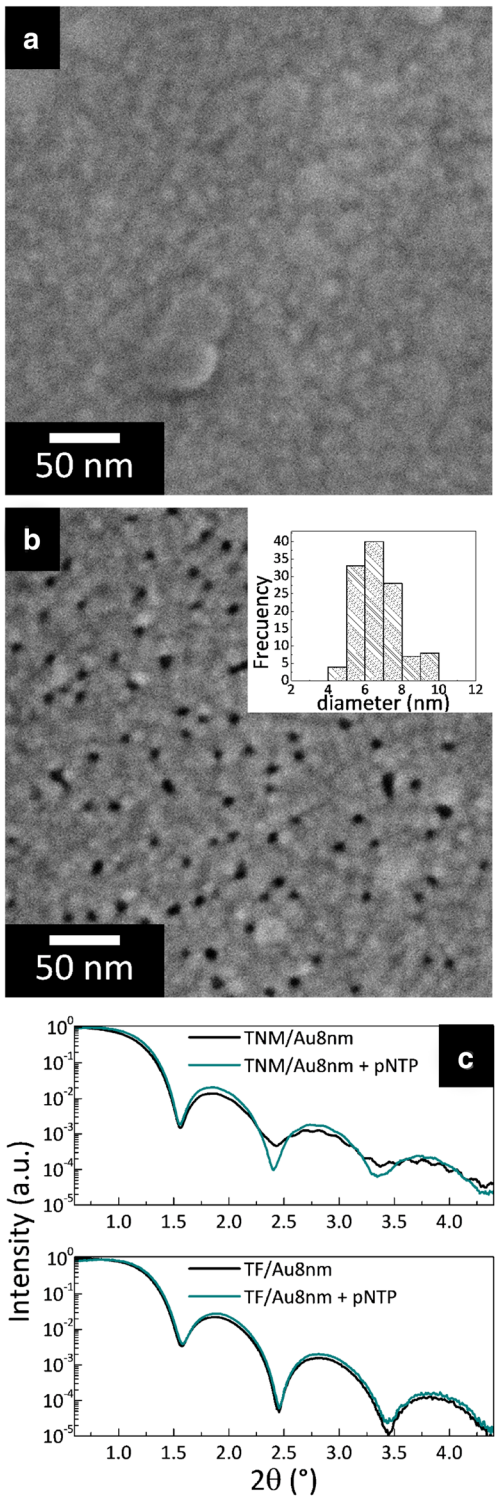

Fig. 3 SEM images after incubation with pNTP of **a** TNM/Au8nm, and **b** TF/Au8nm systems (inset corresponds to hole size distribution). **c** XRR measurements of both systems before and after incubation with pNTP, as indicated in the labels

No significant changes on the Au film are observed in the TNM/Au8nm system. Therefore, the Au film endured despite the inmersion and subsequent washing with an aqueous solution. On the other hand, TF/Au8nm system shows an increase in holes concentrations, from 360 ± 90 to 790 ± 170 holes/μm^2. This increment could be attributed to the loss of very small metallic crystals grown over the pores. Nevertheless, the hole's size and shape remains stable. Moreover, as shown in Fig. 3c, the Au film thickness of both systems did not change after incubation, since observed XRR features are compatible with an 8 nm thick Au film in all cases.

On the other hand, after following the same incubation procedure, samples with a thermal treatment at 300 °C showed a significant change in NPs size distribution. SEM images with their respective NPs size histogram are shown in Fig. 4a, b. For TNM/Au5nm-300 and TF/Au5nm-300 systems, the average NPs diameter decreased to 27 ± 8 nm and 20 ± 10 nm, respectively. This phenomenon is attributed to the fact that only smaller NPs remain attached to TiO_2 surface after incubation. The UV–visible spectra of the samples before and after the incubation can be seen in Fig. 4c. After incubation, the plasmon band shifts towards higher wavelengths. This can be attributed to an increase in refractive index around the NPs due to the effect of pNTP molecules adsorbed onto the metal. Moreover, the presence of plasmonic bands at higher wavelengths can also indicate the partial aggregation of the NPs, due to NPs movement during incubation and subsequent washing. This phenomenon seems to be more evident for TNM/Au5nm-300 system, probably due to the lower surface roughness of the TNM film deposited underneath, that allows higher particle mobility.

The lack of stability of gold NPs over TiO_2 surfaces in presence of aqueous solutions results in non-reproducible and inhomogeneous systems. Interestingly, NPs were also obtained for SF system but they were removed from the surface after incubation, demonstrating that both Au films and Au NPs present lower affinity for SiO_2.

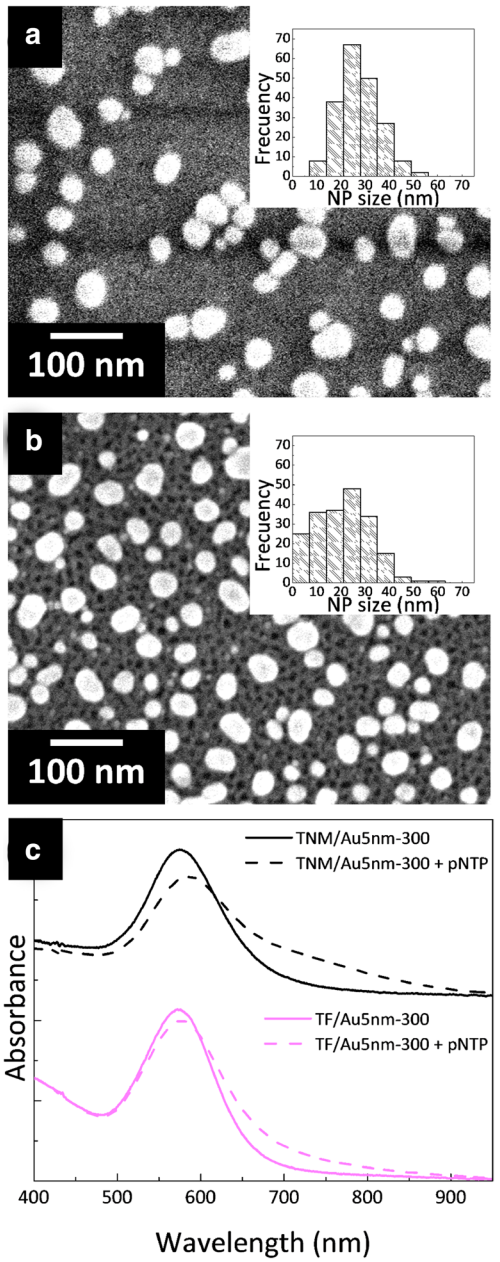

Fig. 4 SEM images after incubation with pNTP of **a** TNM/Au5nm-300, and **b** TF/Au5nm-300 systems. Insets correspond to NPs size distribution. **c** UV–visible spectra of TNM/Au5nm-300 and TF/Au5nm-300 systems before and after incubation with pNTP

3.3 SERS sensing

To test the sensing properties of the synthesized systems, SERS experiments were carried out with the synthesized samples using different molecular probes. Figure 5a displays pNTP SERS spectra obtained using TNM/Au8nm and TF/Au8nm systems. For TNM/Au8nm, no pNTP SERS signal is observed in any interrogated spot, even with acquisition times up to 30 s. On the other hand, pNTP SERS spectrum is observed for every spot tested using the TF/Au8nm system. The intensities of the 1340 cm^{-1} band for each of these 12 different points are presented in Fig. 5b. A spatial standard deviation of 28% was determined for this platform.

These results corroborate the previous observations: there is an important morphological difference between the Au films deposited over porous and non-porous oxide films. While the Au layer formed over the non mesoporous TiO_2 films does not present enough anisotropy or roughness to amplify the Raman spectra of pNTP, the one formed over the porous TiO_2 is SERS active. The results presented

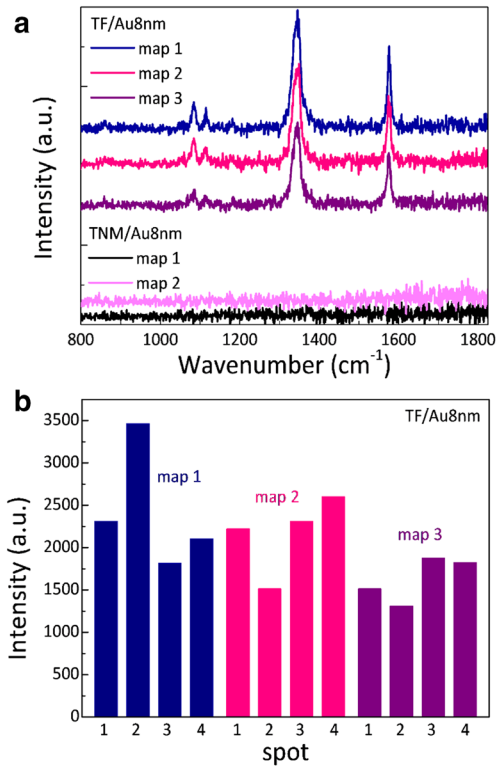

Fig. 5 **a** pNTP SERS spectra obtained using 30 s acquisition time with TNM/Au8nm and TF/Au8nm systems. Each spectra represents the average of data obtained at 4 different points. **b** SERS intensity of the 1340 cm^{-1} band, after background subtraction, for the different spots evaluated in the mappings of the TF/Au8nm platform (30 s acquisition time). The distance between each point in the map is 40 µm

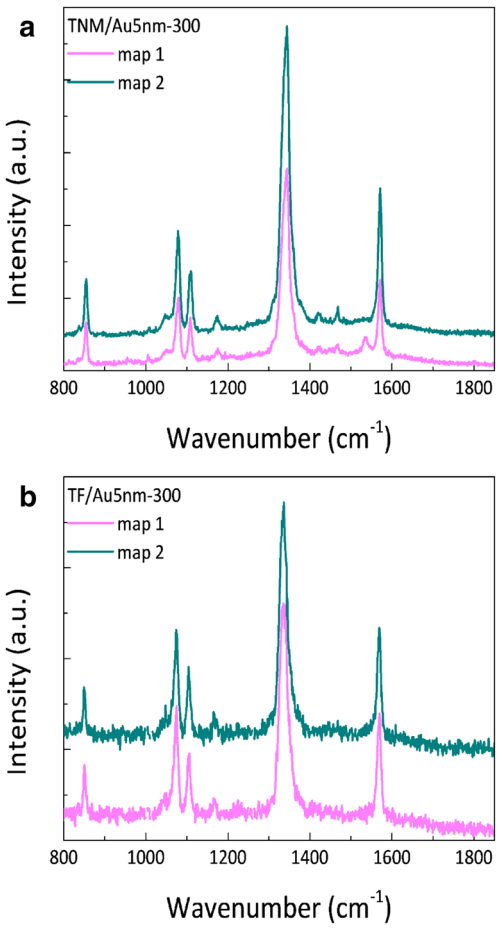

Fig. 6 pNTP SERS spectra obtained using 5 s acquisition time with the systems: **a** TNM/Au5nm-300, and **b** TF/Au5nm-300. Each spectra represents the average of data obtained at 4 different points

here, indicate that the increase in the Raman signal is due to the presence of a semicontinuous Au surface with well distributed holes. This is a key difference with previous works, in which island-type morphologies were obtained over non-mesoporous substrates [48–51].

Moreover, no significant SERS spectra of pNTP was observed when increasing the Au layer thickness to 15 nm, as can be seen in Fig. S4 (SI). This behavior was already described in the literature for continuous Ag coatings [52] and indicates that the roughness of the 15 nm Au layer is not enough to amplify the Raman signal of pNTP.

Figure 6 shows the pNTP SERS spectra obtained using TNM/Au5nm-300 and TF/Au5nm-300 systems. Higher SERS sensitivity is observed for the system with the non-mesoporous oxide film. These two systems present NPs of similar size, that are located at shorter distances for the TNM/Au5nm-300 platform after the incubation with the SERS probe (see Fig. 4). This fact could explain the observed sensitivity differences: close proximity between particles can give rise to hot-spots in which electromagnetic field is amplified, with the consequent higher enhancement of the Raman signal. However, in both cases the pNTP signal intensities were significantly different in each interrogated spot, indicating a poor reproducibility in the SERS signal for these platforms.

In addition, the same systems were tested as sensors for non-thiolate probes, in order to increase the possibility of applying them in real sample analysis. Preliminary results for R6G detection, presented in Fig. S5, demonstrate the feasibility of the approach: the SERS spectra can be visualized after depositing a drop of the probe molecule solution onto the sensor.

It is important to highlight that, when NPs are formed after thermal treatment, SERS intensity is highly increased. This difference corresponds to the observed behavior of the nanostructuration of the Au film due to thermal treatment, the available metallic surface is increased and generates new hot spots in the system. However, the nanostructuration of the surface also increases the spatial inhomogeneity of the SERS signal.

SERS enhancement factors (EF) were estimated, in order to compare the different systems presented here between them and with previously obtained ones. Details on the calculations and approximations used to obtain the values are presented in the SI. Systems after thermal annealing (TF/Au5nm-300 and TNM/Au5nm-300 samples) present EFs in the order of 1 10^6, while TF/Au8nm system presents an EF of 1 10^3. Interestingly, for thermally treated systems the increase in the EF comes with a loss in the spot-to-spot reproducibility.

Previously reported systems in which Au NPs were included inside the pores of mesoporous TiO_2 films present an EF of 4 10^2 [28], comparable with the one obtained for the TF/Au8nm platform. On the other hand, TNM/Au5nm-300 and TF/Au5nm-300 systems present a comparable though higher EF compared to platforms built with anisotropic Au NPs deposited in the substrate-TiO_2 interface (*i.e.* covered by the TiO_2 porous film—EF of 1 10^5). Though it is known that anisotropic Au NPs provide higher electromagnetic field enhancement than isotropic ones, the fact that the systems presented in this work have the NPs in direct contact with the medium increases the plasmonic surface availability. This fact, together with the simplicity of preparation of the systems, makes the platforms presented in this work very promising as SERS sensors.

4 Conclusions

In this work, semicontinuous plasmonic gold films were obtained using a mesoporous TiO_2 films as substrates. This porous TiO_2 film acted as a solid template, allowing the obtention of a structured Au surface, clearly different from the one obtained using non porous TiO_2 as substrate. Interestingly, the Au structuration is observed when films of less than 8 nm thickare deposited; thus, a very small amount of metallic Au is required for sample production. This inexpensive and straightforward platform showed good quality SERS signals, with high point-to-point reproducibility for a thiol containing probe (pNTP). This sensing capability can be explained due to the presence of homogeneously distributed holes in the Au layer, which act as hot-spots. Moreover, the Au thin films sputtered over mesoporous TiO_2 substrates remained stable after incubation with the corrosive pNTP solution, a feature that was not observed when SiO_2 porous films were used as substrates. Thus, no extra metal coating was necessary in order to increase Au adhesivity, simplifying the production procedure.

The SERS signal homogeneity, along with the Au stability and the essentially flat surface of the platforms presented here could aid to develop sensors for the identification of a wide variety of analytes, including those that do not contain thiols as functional groups. In fact, the preliminary results obtained for a non thiolated molecule detection (R6G) indicate that it is possible to directly dry a drop of the analyte solution onto the sensors and obtain a clear SERS signal. In addition, the possibility of achieving quantitative determinations can also be envisioned.

Interestingly, the same systems were subjected to thermal treatment and nude gold spheroidal nanoislands with sizes below 100 nm were obtained. Using this strategy, it was possible to significantly increase SERS sensibility and EF, but signal homogeneity was lost. Thus, depending on the desired application, the best system can be chosen.

Finally, the presented plasmonic film synthesis strategy through ordered mesoporous oxides as templates could be employed to rationally design metallic thin films with plasmonic properties for other technological applications beside the one presented here.

Acknowledgements This work was funded by ANPCyT (PICT 2015-0351, 2017-1133, 2017-3150) and INTERING2015 funded by FUNINTEC. The authors thank to Dr. E. B. Halac for access to Raman equipment and to the personnel of the Clean Room at CAC, CNEA for their help with the gold sputtering. MMZ, PYS and JM acknowledge CONICET for their doctoral fellowships. TP acknowledge FUNINTEC for his undergraduate fellowship.

References

1. Fan M, Andrade GFS, Brolo AG (2011) A review on the fabrication of substrates for surface enhanced Raman spectroscopy and their applications in analytical chemistry. Anal Chim Acta 693:7–25. https://doi.org/10.1016/j.aca.2011.03.002
2. Bell SEJ, Charron G, Cortés E et al (2020) Towards reliable and quantitative surface-enhanced Raman scattering (SERS): from key parameters to good analytical practice. Angew Chem Int Ed 59:5454–5462. https://doi.org/10.1002/anie.201908154
3. Halvorson RA, Vikesland PJ (2010) Surface-enhanced Raman spectroscopy (SERS) for environmental analyses. Environ Sci Technol 44:7749–7755. https://doi.org/10.1021/es101228z
4. Zheng J, He L (2014) Surface-enhanced Raman spectroscopy for the chemical analysis of food. Compr Rev Food Sci Food Saf 13:317–328. https://doi.org/10.1111/1541-4337.12062
5. Chen C, Liu W, Tian S, Hong T (2019) Novel surface-enhanced Raman spectroscopy techniques for DNA. Protein Drug Detect Sens 19:1712. https://doi.org/10.3390/s19071712
6. Fabris L (2016) SERS tags: the next promising tool for personalized cancer detection? ChemNanoMat 2:249–258. https://doi.org/10.1002/cnma.201500221
7. Wang Z, Zong S, Wu L et al (2017) SERS-activated platforms for immunoassay: probes, encoding methods, and applications. Chem Rev 117:7910–7963. https://doi.org/10.1021/acs.chemrev.7b00027
8. Alvarez-Puebla RA, Liz-Marzán LM (2010) SERS-based diagnosis and biodetection. Small 6:604–610. https://doi.org/10.1002/smll.200901820
9. Guselnikova O, Kalachyova Y, Hrobonova K et al (2018) SERS platform for detection of lipids and disease markers prepared using modification of plasmonic-active gold gratings by lipophilic

moieties. Sens Actuators B Chem 265:182–192. https://doi.org/10.1016/j.snb.2018.03.016
10. Kalachyova Y, Erzina M, Postnikov P et al (2018) Flexible SERS substrate for portable Raman analysis of biosamples. Appl Surf Sci 458:95–99. https://doi.org/10.1016/j.apsusc.2018.07.073
11. Premasiri WR, Chen Y, Fore J et al (2018) Chapter 10 - SERS biomedical applications: diagnostics, forensics, and metabolomics. In: Laane J (ed) Frontiers and Advances in Molecular Spectroscopy. Elsevier, Amsterdam, pp 327–367
12. Álvarez-Puebla RA, Liz-Marzán LM (2010) Environmental applications of plasmon assisted Raman scattering. Energy Environ Sci 3:1011–1017. https://doi.org/10.1039/C002437F
13. Alvarez-Puebla RA, Liz-Marzán LM (2012) SERS detection of small inorganic molecules and ions. Angew Chem Int Ed 51:11214–11223. https://doi.org/10.1002/anie.201204438
14. McNay G, Eustace D, Smith WE et al (2011) Surface-enhanced Raman scattering (SERS) and surface-enhanced resonance Raman scattering (SERRS): a review of applications. Appl Spectrosc 65:825–837. https://doi.org/10.1366/11-06365
15. Langer J, Jimenez de Aberasturi D, Aizpurua J et al (2020) Present and future of surface-enhanced Raman scattering. ACS Nano 14:28–117. https://doi.org/10.1021/acsnano.9b04224
16. Schlücker S (2014) Surface-enhanced Raman spectroscopy: concepts and chemical applications. Angew Chem Int Ed 53:4756–4795. https://doi.org/10.1002/anie.201205748
17. Bekana D, Liu R, Amde M, Liu J-F (2017) Use of polycrystalline ice for assembly of large area au nanoparticle superstructures as SERS substrates. ACS Appl Mater Interfaces 9:513–520. https://doi.org/10.1021/acsami.6b15378
18. Mehrvar L, Sadeghipari M, Tavassoli SH, Mohajerzadeh S (2017) Surface-enhanced Raman spectroscopy of dye molecules on Ag-modified silicon nanowire substrates: influence of photoinduced probe degradation on enhancement factors. J Raman Spectrosc 48:1171–1181. https://doi.org/10.1002/jrs.5186
19. Rodriguez RD, Sheremet E, Nesterov M et al (2018) Aluminum and copper nanostructures for surface-enhanced Raman spectroscopy: A one-to-one comparison to silver and gold. Sens Actuators B Chem 262:922–927. https://doi.org/10.1016/j.snb.2018.02.006
20. Kessentini S, Barchiesi D, D'Andrea C et al (2014) Gold dimer nanoantenna with slanted gap for tunable LSPR and improved SERS. J Phys Chem C 118:3209–3219. https://doi.org/10.1021/jp409844y
21. Zhou X, Zhou F, Liu H et al (2013) Assembly of polymer–gold nanostructures with high reproducibility into a monolayer film SERS substrate with 5 nm gaps for pesticide trace detection. Analyst 138:5832–5838. https://doi.org/10.1039/C3AN00914A
22. Sharma B, Frontiera RR, Henry A-I et al (2012) SERS: Materials, applications, and the future. Mater Today 15:16–25. https://doi.org/10.1016/S1369-7021(12)70017-2
23. Lee S, Kim J, Yang H et al (2019) Particle-in-a-frame nanostructures with interior nanogaps. Angew Chem Int Ed 58:15890–15894. https://doi.org/10.1002/anie.201908291
24. Innocenzi P, Malfatti L (2019) Mesoporous materials as platforms for surface-enhanced Raman scattering. TrAC Trends Anal Chem 114:233–241. https://doi.org/10.1016/j.trac.2019.02.031
25. Soler-Illia GJdAA, Sanchez C, Lebeau B, Patarin J (2002) Chemical strategies to design textured materials: from microporous and mesoporous oxides to nanonetworks and hierarchical structures. Chem Rev 102(4093):4138. https://doi.org/10.1021/cr0200062
26. Malfatti L, Falcaro P, Marmiroli B et al (2011) Nanocomposite mesoporous ordered films for lab-on-chip intrinsic surface enhanced Raman scattering detection. Nanoscale 3:3760–3766. https://doi.org/10.1039/C1NR10404G
27. Wolosiuk A, Tognalli NG, Martínez ED et al (2014) silver nanoparticle-mesoporous oxide nanocomposite thin films: a platform for spatially homogeneous SERS-active substrates with enhanced stability. ACS Appl Mater Interfaces 6:5263–5272. https://doi.org/10.1021/am500631f
28. Zalduendo MM, Langer J, Giner-Casares JJ et al (2018) Au Nanoparticles-mesoporous TiO2 thin films composites as SERS sensors: A systematic performance analysis. J Phys Chem C 122:13095–13105. https://doi.org/10.1021/acs.jpcc.8b01444
29. Steinberg PY, Zalduendo MM, Giménez G et al (2019) TiO2 mesoporous thin film architecture as a tool to control Au nanoparticles growth and sensing capabilities. Phys Chem Chem Phys 21:10347–10356. https://doi.org/10.1039/C9CP01896D
30. López-Puente V, Abalde-Cela S, Angelomé PC et al (2013) Plasmonic mesoporous composites as molecular sieves for SERS detection. J Phys Chem Lett 4:2715–2720. https://doi.org/10.1021/jz4014085
31. López-Puente V, Angelomé PC, Soler-Illia GJAA, Liz-Marzán LM (2015) Selective SERS sensing modulated by functionalized mesoporous films. ACS Appl Mater Interfaces 7:25633–25640. https://doi.org/10.1021/acsami.5b10543
32. Bodelón G, Montes-García V, López-Puente V et al (2016) Detection and imaging of quorum sensing in Pseudomonas aeruginosa biofilm communities by surface-enhanced resonance Raman scattering. Nat Mater 15:1203–1211. https://doi.org/10.1038/nmat4720
33. Xu Y, Kutsanedzie FYH, Hassan M et al (2020) Mesoporous silica supported orderly-spaced gold nanoparticles SERS-based sensor for pesticides detection in food. Food Chem 315:126300. https://doi.org/10.1016/j.foodchem.2020.126300
34. Panarin AYu, Chirvony VS, Kholostov KI et al (2009) Formation of SERS-active silver structures on the surface of mesoporous silicon. J Appl Spectrosc 76:280–287. https://doi.org/10.1007/s10812-009-9175-1
35. Mura S, Greppi G, Innocenzi P et al (2013) Nanostructured thin films as surface-enhanced Raman scattering substrates. J Raman Spectrosc 44:35–40. https://doi.org/10.1002/jrs.4151
36. Murai S, Uno S, Kamakura R et al (2015) Plasmonic mesostructures prepared by oriented mesoporous materials as a template. ECS Trans 69:117. https://doi.org/10.1149/06902.0117ecst
37. Murai S, Uno S, Kamakura R et al (2016) Plasmonic mesostructures with aligned hotspots on highly oriented mesoporous silica films. Opt Mater Express 6:2824–2833. https://doi.org/10.1364/OME.6.002824
38. Wang Y-W, Kao K-C, Wang J-K, Mou C-Y (2016) Large-scale uniform two-dimensional hexagonal arrays of gold nanoparticles templated from mesoporous silica film for surface-enhanced Raman spectroscopy. J Phys Chem C 120:24382–24388. https://doi.org/10.1021/acs.jpcc.6b08116
39. Long Y, Wang X, Chen D et al (2016) Intense and stable surface-enhanced Raman scattering from Ag@mesoporous SiO2 film. J Lumin 177:387–393. https://doi.org/10.1016/j.jlumin.2016.05.024
40. Jiang T, Wang X, Zhou J et al (2016) Hydrothermal synthesis of Ag@MSiO2@Ag three core–shell nanoparticles and their sensitive and stable SERS properties. Nanoscale 8:4908–4914. https://doi.org/10.1039/C6NR00006A
41. Huang Z, Meng G, Huang Q et al (2010) Improved SERS performance from Au nanopillar arrays by abridging the pillar tip spacing by Ag sputtering. Adv Mater 22:4136–4139. https://doi.org/10.1002/adma.201001179
42. D'Andrea C, Fazio B, Gucciardi PG et al (2014) SERS enhancement and field confinement in nanosensors based on self-organized gold nanowires produced by Ion-beam sputtering. J Phys Chem C 118:8571–8580. https://doi.org/10.1021/jp5007236

43. Zhao X, Wen J, Zhang M et al (2017) Design of hybrid nanostructural arrays to manipulate SERS-active substrates by nanosphere lithography. ACS Appl Mater Interfaces 9:7710–7716. https://doi.org/10.1021/acsami.6b14008
44. Dai Z, Wang G, Xiao X et al (2014) Obviously angular, cuboid-shaped TiO2 nanowire arrays decorated with Ag nanoparticle as ultrasensitive 3D surface-enhanced Raman scattering substrates. J Phys Chem C 118:22711–22718. https://doi.org/10.1021/jp507601p
45. Cacciato G, Ruffino F, Zimbone M et al (2016) Au thin films nanostructuration on polycrystalline anatase and rutile TiO2 substrates towards photocatalytic applications. Mater Sci Semicond Process 42:40–44. https://doi.org/10.1016/j.mssp.2015.07.074
46. Kossoy A, Merk V, Simakov D et al (2015) Optical and structural properties of ultra-thin gold films. Adv Opt Mater 3:71–77. https://doi.org/10.1002/adom.201400345
47. Bonyár A, Csarnovics I, Veres M et al (2018) Investigation of the performance of thermally generated gold nanoislands for LSPR and SERS applications. Sens Actuators B Chem 255:433–439. https://doi.org/10.1016/j.snb.2017.08.063
48. Pavaskar P, Hsu I-K, Theiss J et al (2013) A microscopic study of strongly plasmonic Au and Ag island thin films. J Appl Phys 113:034302. https://doi.org/10.1063/1.4775784
49. Andrikaki S, Govatsi K, N. Yannopoulos S, et al (2018) Thermal dewetting tunes surface enhanced resonance Raman scattering (SERRS) performance. RSC Adv 8:29062–29070. https://doi.org/10.1039/C8RA05451G
50. Khlebtsov BN, Khanadeev VA, Panfilova EV et al (2015) Gold Nanoisland Films as Reproducible SERS Substrates for Highly Sensitive Detection of Fungicides. ACS Appl Mater Interfaces 7:6518–6529. https://doi.org/10.1021/acsami.5b01652
51. Fusco Z, Bo R, Wang Y et al (2019) Self-assembly of Au nanoislands with tuneable organized disorder for highly sensitive SERS. J Mater Chem C 7:6308–6316. https://doi.org/10.1039/C9TC01231A
52. Liszewska M, Budner B, Norek M et al (2019) Revisiting semicontinuous silver films as surface-enhanced Raman spectroscopy substrates. Beilstein J Nanotechnol 10:1048–1055. https://doi.org/10.3762/bjnano.10.105
53. Soler-Illia GJAA, Angelomé PC, Fuertes MC et al (2012) Critical aspects in the production of periodically ordered mesoporous titania thin films. Nanoscale 4:2549–2566. https://doi.org/10.1039/C2NR11817C
54. Angelomé PC, Fuertes MC, Soler-Illia GJaA (2006) Multifunctional, multilayer, multiscale: integrative synthesis of complex macroporous and mesoporous thin films with spatial separation of porosity and function. Adv Mater 18:2397–2402. https://doi.org/10.1002/adma.200600439
55. Brinker CJ, Lu Y, Sellinger A, Fan H (1999) Evaporation-induced self-assembly: nanostructures made easy. Adv Mater 11:579–585. https://doi.org/10.1002/(SICI)1521-4095(199905)11:7<579:AID-ADMA579>3.0.CO;2-R
56. Fuertes MC, Barrera MP, Plá J (2012) Sorption and optical properties of sol–gel thin films measured by X-Ray reflectometry and ellipsometric porosimetry. Thin Solid Films 520:4853–4862. https://doi.org/10.1016/j.tsf.2012.03.018
57. Crepaldi EL, Soler-IlliaGrosso GJdAAD et al (2003) Controlled formation of highly organized mesoporous titania thin films: from mesostructured hybrids to mesoporous nanoanatase TiO2. J Am Chem Soc 125:9770–9786. https://doi.org/10.1021/ja030070g
58. Malinský P, Slepička P, Hnatowicz V, Švorčík V (2012) Early stages of growth of gold layers sputter deposited on glass and silicon substrates. Nanoscale Res Lett 7:241. https://doi.org/10.1186/1556-276X-7-241
59. Švorčík V, Siegel J, Šutta P et al (2011) Annealing of gold nanostructures sputtered on glass substrate. Appl Phys A 102:605–610. https://doi.org/10.1007/s00339-010-6167-1
60. Švorčík V, Kvítek O, Lyutakov O et al (2011) Annealing of sputtered gold nano-structures. Appl Phys A 102:747–751. https://doi.org/10.1007/s00339-010-5977-5
61. Shinotsuka K, Shen L, Dai K et al (2019) Automatic fabrication of high-sensitive SERS-active nanogaps between Au sea and Au islands. Jpn J Appl Phys 58:032001. https://doi.org/10.7567/1347-4065/aafddf
62. Korotcenkov G, Brinzari V, Cho BK (2016) Conductometric gas sensors based on metal oxides modified with gold nanoparticles: a review. Microchim Acta 183:1033–1054. https://doi.org/10.1007/s00604-015-1741-z
63. Alberti S, Steinberg PY, Giménez G et al (2019) Chemical stability of mesoporous oxide thin film electrodes under electrochemical cycling: from dissolution to stabilization. Langmuir 35:6279–6287. https://doi.org/10.1021/acs.langmuir.9b00224